ACTA ONCOLOGICA, 2017
VOL. 56, NO. 11, 1465–1471
https://doi.org/10.1080/0284186X.2017.1372625

Taylor & Francis
Taylor & Francis Group

ORIGINAL ARTICLE

A comparison of relative proton stopping power measurements across patient size using dual- and single-energy CT

Gregory Michalak[a], Vicki Taasti[b], Bernhard Krauss[c], Amanda Deisher[d], Ahmed Halaweish[e] and Cynthia McCollough[a]

[a]Department of Radiology, Mayo Clinic, Rochester, MN, USA; [b]Department of Medical Physics, Aarhus University Hospital, Aarhus, Denmark; [c]Siemens Healthineers, Forchheim, Germany; [d]Department of Radiation Oncology, Mayo Clinic, Rochester, MN, USA; [e]Siemens Healthineers, Malvern, PA, USA

ABSTRACT

Purpose: To evaluate the accuracy and precision across phantom size of a dual-energy computed tomography (DECT) technique used to calculate relative proton stopping power (SPR) in tissue-simulating materials and a silicone implant relative to conventional single-energy CT (SECT).

Material and methods: A 32 cm lateral diameter (CIRS model 062M, Norfolk, Virginia) electron density phantom containing inserts which simulated the chemical composition of eight tissues in a solid-water background was scanned using SECT and DECT. A liquid water insert was included to confirm CT number accuracy. All materials were also placed in four water tanks, ranging from 15 to 45 cm in lateral width and scanned using DECT and SECT. A silicone breast implant was scanned in the same water phantoms. SPR values were calculated based on commercial software (syngo CT Dual Energy, Siemens Healthcare GmbH) and compared to reference values derived from proton beam measurements. Accuracy and precision were quantified across phantom size using percent error and standard deviation. Graphical and regression analysis were used to determine whether SECT or DECT was superior in estimating SPR across phantom size.

Results: Both DECT and SECT SPR data resulted in good agreement with the reference values. Percent error was ±3% for both DECT and SECT in all materials except lung and dense bone. The coefficient of variation (CV) across materials and phantom sizes was 1.12% for SECT and 0.96% for DECT. Material-specific regression and graphical analysis did not reveal size dependence for either technique but did show reduced systematic bias with DECT for dense bone and liver. Mean percent error in SPR for the implant was reduced from 11.46% for SECT to 0.49% for DECT.

Conclusions: We demonstrate the superior ability of DECT to mitigate systematic bias in bones and liver and estimate SPR in a silicone breast implant.

ARTICLE HISTORY
Received 21 June 2017
Accepted 17 August 2017

Introduction

Computed tomography is the preferred modality for acquisition of patient images for radiation therapy planning [1]. Particularly with proton beam therapy, the determination of the chemical composition of the tissues in the beam path is essential for accurately and precisely predicting dose delivery to both the target and collateral tissues. Schneider et al. [2] described a method for determining the ratio of the proton stopping power of a given material to that of water (SPR) using single-energy CT (SECT). This method, referred to as the stoichiometric method, entails a three step process. In step 1, the CT system is parameterized using CT numbers from scans of tissue surrogates of known chemical composition and physical density. In step 2, the predicted CT numbers and SPR's of various tissues are determined using the CT system parameters determined in step 1 and the Bethe equation, respectively. Elemental data for a wide array of tissue types are available in the literature [3–6]. Lastly, step 3 entails generating a piecewise linear fit that maps CT number to SPR. Yang et al. [7] performed a systematic analysis of the sources of error in the stoichiometric technique and found that patient size contributed a large proportion of the uncertainty in both CT number and SPR.

One shortcoming of the stoichiometric method is that it is assumed that materials with the same CT number also have the same SPR. However, SPR is a function of both the proton energy and the chemical properties of the material in which the proton is traveling [8]. These properties include the relative electron density, ρ_e, and the logarithm of the mean ionization energy of the material, ln(I). Both parameters can be estimated if the attenuation of the material is known at two energies. This type of measurement is possible using dual energy CT (DECT) [9].

Recently, software has been developed that can directly estimate ρ_e and the effective atomic number (Z_{eff}) of tissues using DECT data [10]. Subsequently, ln(I) can be determined using empirical processes if Z_{eff} is known [9]. In this way, DECT can be used to measure not only the dominant contribution to the SPR from electron density, but also the next-to leading contribution from chemical composition.

CONTACT Cynthia McCollough mccollough.cynthia@mayo.edu Department of Radiology, Mayo Clinic, Rochester, MN, USA

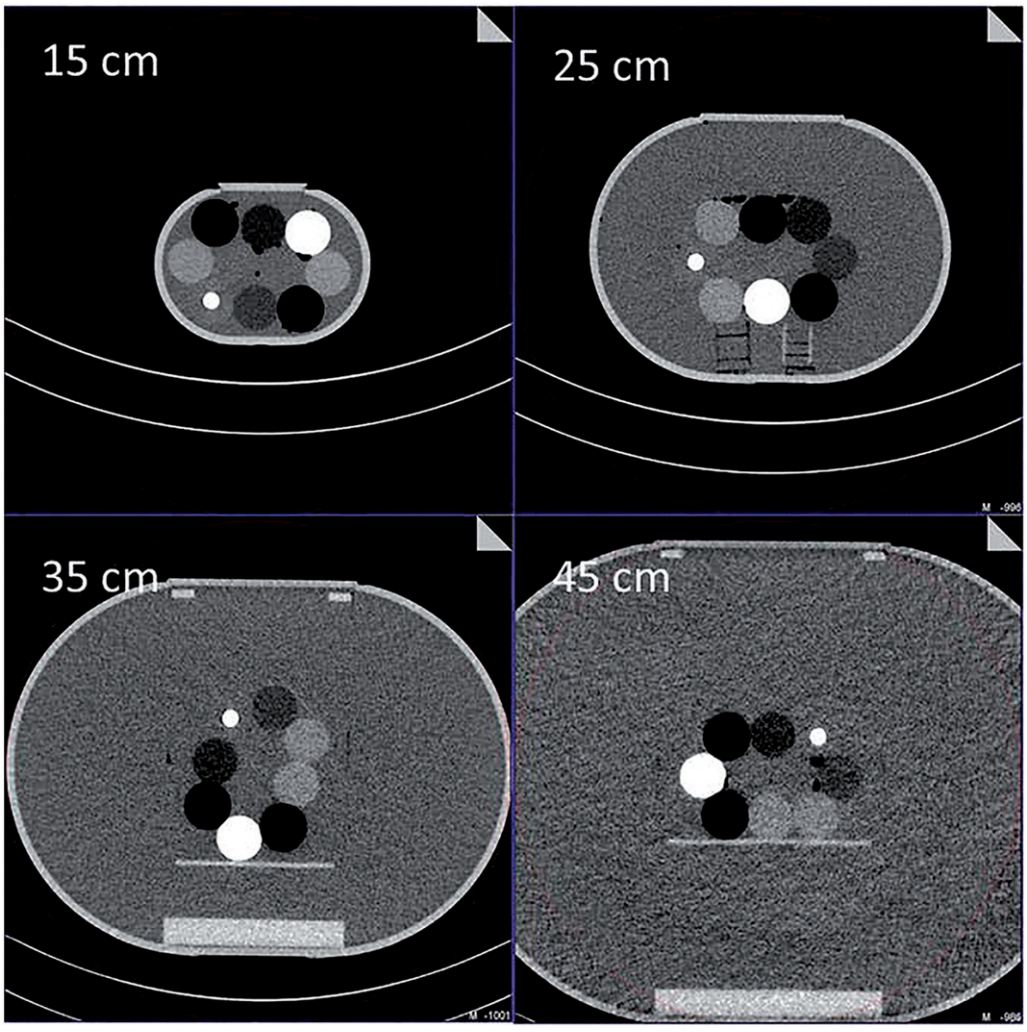

Figure 1. Four water tanks containing the bundle of tissue-simulating materials including two solid water inserts in the middle.

Furthermore, SECT may be less accurate in specific clinical situations. For example, it has been demonstrated that DECT can be used to reduce the variation in CT number that occurs across patient size due to beam hardening [11] and reduce overall image noise [12]. Bar, et al. [13] has outlined several robust techniques of using DECT data to accurately characterize tissue SPR using both direct and empirical approaches. It is possible, therefore, that this DECT technique could be used in proton therapy planning to make more accurate SPR measurements across the spectrum of patient sizes. In addition, DECT can distinguish between materials with same CT number but different SPR (e.g., soft tissue vs. silicone implants). The aim of this study was to compare SPR estimates derived from both SECT and DECT across phantom size to determine if size dependence and/or systematic bias is reduced with the current DECT method.

Material and methods

Electron density phantom and CT scans

Tissue inserts from a commercial electron density phantom (CIRS model 062M, Norfolk, Virginia, USA) were scanned using both SECT and DECT routine abdomen protocols on a third-generation dual-source CT system (SOMATOM Force, Siemens Healthcare, Forchhiem, Germany). Each insert simulated the electron density of one of eight different tissues (lung inhale, lung exhale, adipose, breast, muscle, liver, trabecular bone and dense bone) and had lengths of approximately 80 mm and diameters between 30 and 32 mm depending on the longitudinal location (i.e., they are slightly tapered). These inserts were arranged in a bundle around two solid water inserts (same material that comprised the background in the commercial product) having the same physical dimensions as the tissue inserts and placed in the center of four torso-shaped water tanks ranging in lateral width from 15 to 45 cm in 10 cm increments (Figure 1) for CT imaging. Each phantom was first scanned with the SECT protocol, then a dose-matched DECT protocol. The SECT protocol used a tube potential of 120 kV and a quality reference mAs (QRM) of 180. The DECT protocol used a tube potential pair of 90/150Sn, and the tube current for the DE protocol was adjusted so the dose (as represented by $CTDI_{vol}$) delivered to the phantom matched that delivered during the SECT scan. Both SECT and DECT data acquisitions used a detector collimation of 192×0.6 mm. All images were reconstructed using a quantitative semismooth kernel (Qr40) and a slice thickness of 1.5 mm and increment of 1 mm.

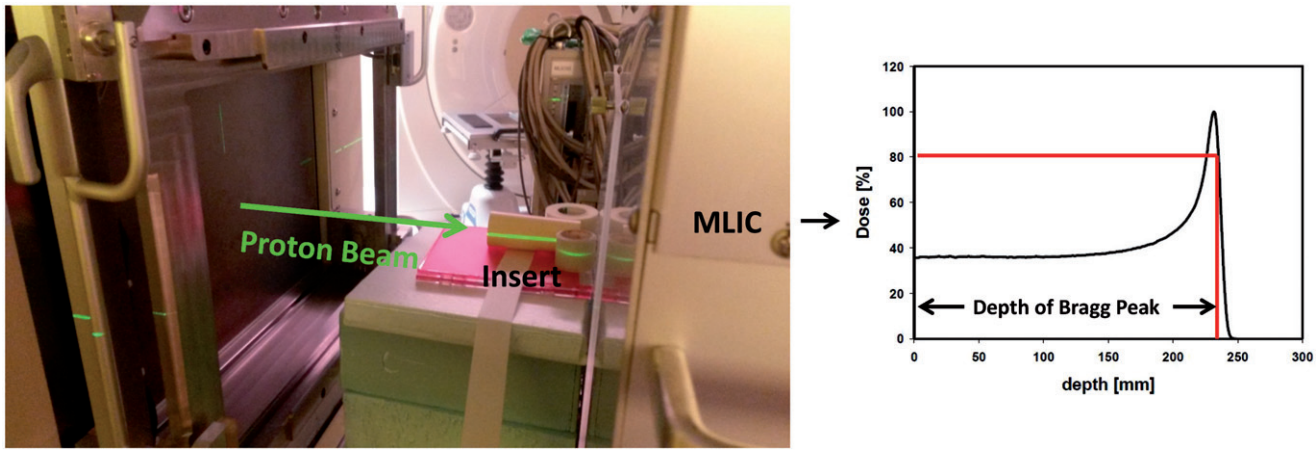

Figure 2. Setup for acquisition of reference relative stopping power (SPR) for each tissue insert.

DECT and SECT scans were also performed on the 25, 35 and 45 cm water tanks after insertion of a silicone breast implant. The 15-cm tank was excluded because it was too small to hold the implant.

SPR measurements using a proton beam

To obtain reference values for SPR in each insert and the silicone breast implant, proton beam measurements were performed (Figure 2). Prior to proton beam irradiation, SECT images of each tissue insert (excluding the silicone implant) were loaded into a Monte Carlo program which simulated their irradiation using a proton beam having a circular cross section and a Gaussian intensity profile having a sigma of 2 mm measured in air. The protons had a trajectory along the long axis of each material. The simulations resulted in all protons entering and exiting the proximal and distal flat surfaces of each insert, which ensured that attenuation of the beam was due to passing through a homogeneous medium. The materials were then irradiated with a proton beam having a kinetic energy of 185.2 MeV and a beam profile identical to that simulated. . The water equivalent thickness (WET) of the materials was measured using a customized multilayer ionization chamber (MLIC) (Hitachi, Hitachi, Japan). The range of the proton beam was measured at the 80% distal fall-off (Figure 2) with a precision of 0.2 mm. Each cylinder was placed in the beam, causing a shift in the Bragg peak, which was equal to the WET of the insert. The physical lengths of the inserts were each measured using a digital caliper. SPR was determined by calculating the ratio of the shift in the Bragg peak to the measured length of the insert:

$$\mathrm{SPR}_{\mathrm{meas}} = \frac{R_{80,\mathrm{air}} - R_{80}}{L} \quad (1)$$

where R_{80} is the range of the proton beam at 80% distal fall-off when passing through the measured material and $R_{80,\mathrm{air}}$ is this number when not having a material in the beam path before the MLIC detector. L is the length of the material.

For the silicone implant, a 228.5 MeV proton beam with the same spot size was used. Since the silicone implant was not a rigid object with flat surfaces, it was affixed between two Plexiglas sheets while in the beam in order to produce a uniform medium of known thickness.

Water measurements

To verify CT number accuracy in each water tank, mean CT number was measured in liquid water in the 120 kV SE images and a DE image set produced using a weighted summation of the high and low kV images. The weighting ratio was 0.6 for the low kV images and 0.4 for the low kV images, which resulted in CT numbers similar to those seen in the 120 kV images. Circular regions of interest (ROI's) were drawn in five locations around the tissue insert bundle in the water background and their mean CT number was calculated.

SPR calculations

DECT images of both the CIRS phantom and the water tanks were loaded on to an external workstation and were processed using a commercial software application for the estimation of ρ_e and Z_{eff} (Rho-Z, syngo.CT Dual Energy, syngo.via, Siemens Healthcare GmbH, Erlangen, Germany). The Rho-Z software reports scaled ρ_e images, and therefore, ρ_e was calculated using the following equation:

$$\rho_e = 0.001 \cdot \rho_{e,Rho-Z} + 1 \quad (2)$$

where $\rho_{e,Rho-Z}$ is the mean scaled ρ_e over the measured ROI. This provided the electron density of the material relative to water (i.e. if $\rho_{e,Rho-Z} = 0$, $\rho_e = 1$). The value for Z_{eff} was reported directly by the software.

For SECT images, ROI's were drawn in the same manner as for DE. SECT SPR estimates were made using the clinical calibration curve used at Mayo Clinic for proton therapy planning using SECT to convert the measured CT numbers to SPR. The curve was developed using the stoichiometric method described by Schneider et al. [2] and consisted of measurements taken from both the CIRS inserts and a variety of other materials commonly encountered in proton treatment scenarios. It consisted of data points that were fit by line segments (Figure 3). The SPR estimates were determined by mapping the CT numbers to the line segment that

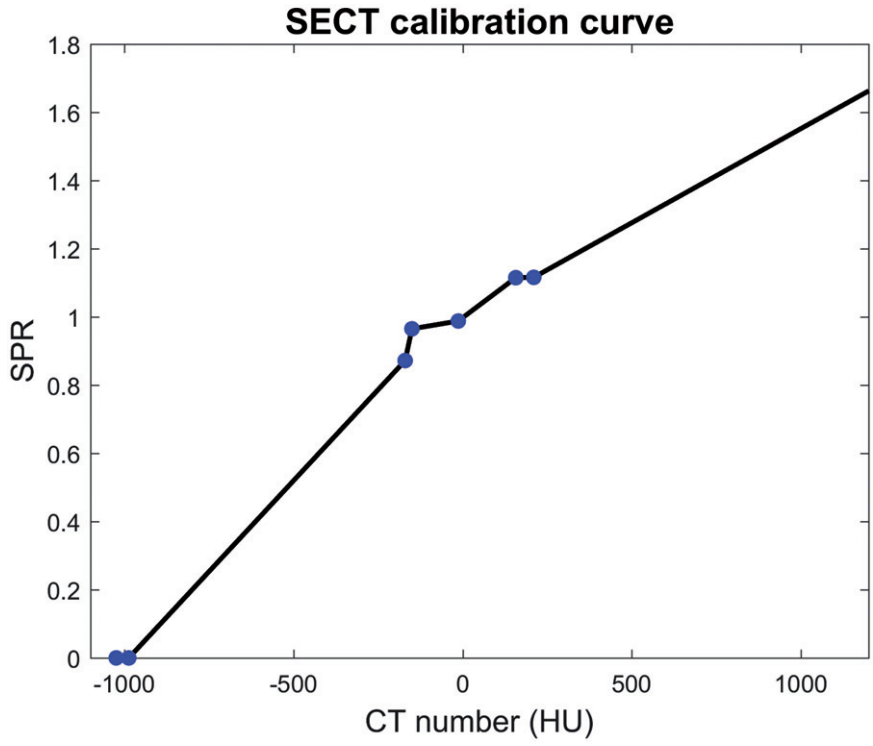

Figure 3. Calibration curve used to map SECT numbers to electron density.

connected the two calibration curve data points above and below it.

For the DECT SPR estimates, we calculated the SPR based on the output from the Rho-Z software for ρ_e and Z_{eff} using the Bethe equation without correction terms (Equation (3) in Schneider et al. [2]). For the calculations, we used an initial kinetic energy of the proton beam to be 185.2 MeV, and for the mean excitation energy of water, we used 75 eV [2]. For the SPR estimates of the silicone implant, the energy of the proton beam was set to 228.5 MeV.

To calculate the SPR from the Bethe equation, a conversion of the Z_{eff} estimates to ln(I) values was needed. For this conversion, we used a piecewise linear fit, as proposed by Yang et al. [9]. To fit this curve, we used the same 34 reference human tissues as used by Yang et al.; however, the thyroid tissue was excluded from the fitting process, as done in the original article.

For the calculation of Z_{eff} for the reference human tissues, we used the following equation [14,15]:

$$Z_{eff} = \left(\frac{\sum_i^N w_i \frac{Z_i^{\beta+1}}{A_i}}{\sum_i^N w_i \frac{Z_i}{A_i}} \right)^{1/\beta} \quad (3)$$

Here, w_i is the mass fraction, Z_i is the atomic number and A_i is the elemental mass of element i in the compound material. We used a value of 3.1 for the β-exponent [10] and then calculated Z_{eff} values for 34 reference human tissues.

To calculate the ln(I) values for the reference human tissues, we used the Bragg additivity rule (Equation (4) of Schneider et al. [2]) and the mean excitation energies, I, for the individual elements taken from Table 2.8 and 2.11 in the ICRU49 report [5,16]. We then made a piecewise linear fit between Z_{eff} and ln(I) for the reference human tissues (Figure 4). The division point between soft and bone tissues was set at Z_{eff} =8.7. These linear fits were then used to estimate the ln(I) values for the CIRS inserts and the breast implant from their measured Z_{eff}. Based on these estimated ln(I) values and their measured ρ_e from the Rho-Z software, SPR was calculated using the Bethe equation.

Since the Rho-Z software did not report a value for Z_{eff} for the two lung inserts, we were not able to estimate the ln(I) based on the regression model. However, since the ln(I) value of lung is close to the value for water, we decided to set the estimated SPR for the lung inserts equal to their measured ρ_e.

Accuracy of SPR estimates in each material and phantom size was determined by calculating the percent error relative to the reference SPR values. The coefficient of variation (CV) across phantom size for each material was determined by finding the mean and standard deviation (SD) in relevant ROI's and then calculating the CV as SD/mean × 100%. To determine the degree to which size affected SPR measurements, and whether the use of DECT reduced this effect, multivariate linear regression models were generated for the percent error data including all materials, and for each individual material. Each model used both size, technique (DECT or SECT), and their interaction:

$$\varepsilon = \beta_0 + \beta_1 \cdot technique + \beta_2 \cdot size + \beta_3 \cdot (technique \cdot size) \quad (4)$$

where ε is the percent error between the reference SPR and the measured SPR. The technique regression variable was defined as a Boolean value (1 or 0). Therefore, the regression models for DECT and SECT were as follows:

$$\varepsilon_{DE} = \beta_0 + \beta_1 + size \cdot (\beta_2 + \beta_3) \quad (5)$$

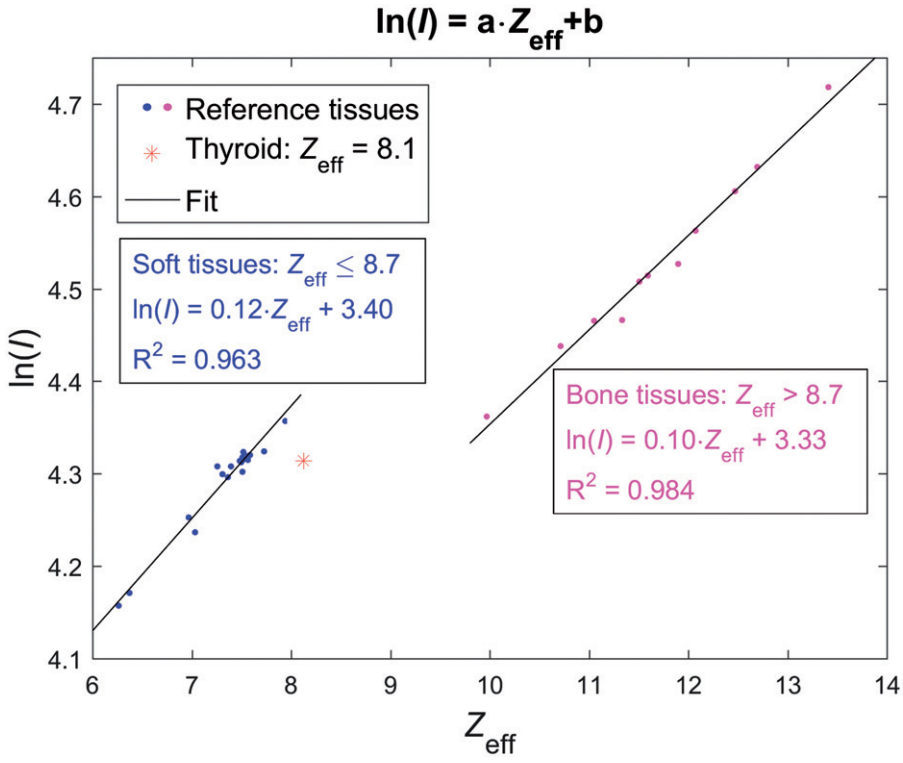

Figure 4. Piecewise linear fit used to convert Z_{eff} into ln(I) estimates.

$$\varepsilon_{SE} = \beta_0 + \beta_2 \cdot size \quad (6)$$

A significant β_3 (interaction term) would indicate that there was variance in the data due to interaction between phantom size and the technique used (DECT vs. SECT). A significant β_1 (technique term) would indicate that there was potentially a systematic shift (bias) in the data due to the technique used. Assessment of dependence on phantom size and bias was also performed by graphing the percent error for each material as a function of size and fitting these data to a linear regression model.

Results

Water measurements

Before analyzing the measurements in each tissue insert, water CT number was first verified.

For SECT, these measurements were −1, −4, −5 and −4 HU, and for DE, they were 2, −2, −2 and −7 HU in the 15, 25, 35 and 45 cm phantoms, respectively. The DE measurement in the 45-cm tank was outside the typical CT number range for water (±5 HU) but was considered acceptable given that the tank was much larger than the 32 cm phantom used for daily system QA.

SPR measurements in the CIRS inserts

Both SECT and DECT estimates of SPR showed good agreement and low percent error across phantom size. Figure 5 shows the percent error in SPR as a function of phantom size for each of the nine materials. In general, the percent error tended to be independent of phantom size and ranged between −3% and 3% for both SECT and DECT, with the exception of the lungs and dense bone. This is illustrated by the flat regression lines for soft tissues and water, and the sloped lines for lungs and dense bone. The mean absolute percent error (accuracy) across patient size for SECT ranged from 0% in breast to 4.39% in lung (exhale). For DECT, this ranged from 0.18% in breast to 6.12% in lung (inhale). The CV ranged from nearly 0% in adipose tissue and breast to 4.1% in lung (inhale) for SECT, and from 0.29% in breast to 3.64% in lung (inhale) for DECT. The mean CV for SECT and DECT was 1.12% and 0.96%, respectively. Material-specific electron density mean, SD, and CV are reported in Table 1.

The multiple linear regression model including the data from all tissue types did not result in a significant interaction between scan technique and phantom size. The technique term was also deemed nonsignificant, meaning that no significant difference was found for the accuracy between SECT and DECT. When the same analysis was performed on tissue-specific data, again no significant interaction terms were detected. Significant technique terms were detected in the regression models for dense bone ($p = .003$) and liver ($p = .007$) which may be related to tolerances of the used phantom materials or systematic differences of the two approaches.

SPR measurements in the silicone implant

SPR for the silicone implant as determined by proton beam measurements was 0.934. Using the SECT calibration curve, the SPR estimates were 1.054, 1.04 and 1.029 in the 25, 35 and 45 cm phantoms, respectively. These estimates resulted in errors of 12.85%, 11.35% and 10.17%, respectively.

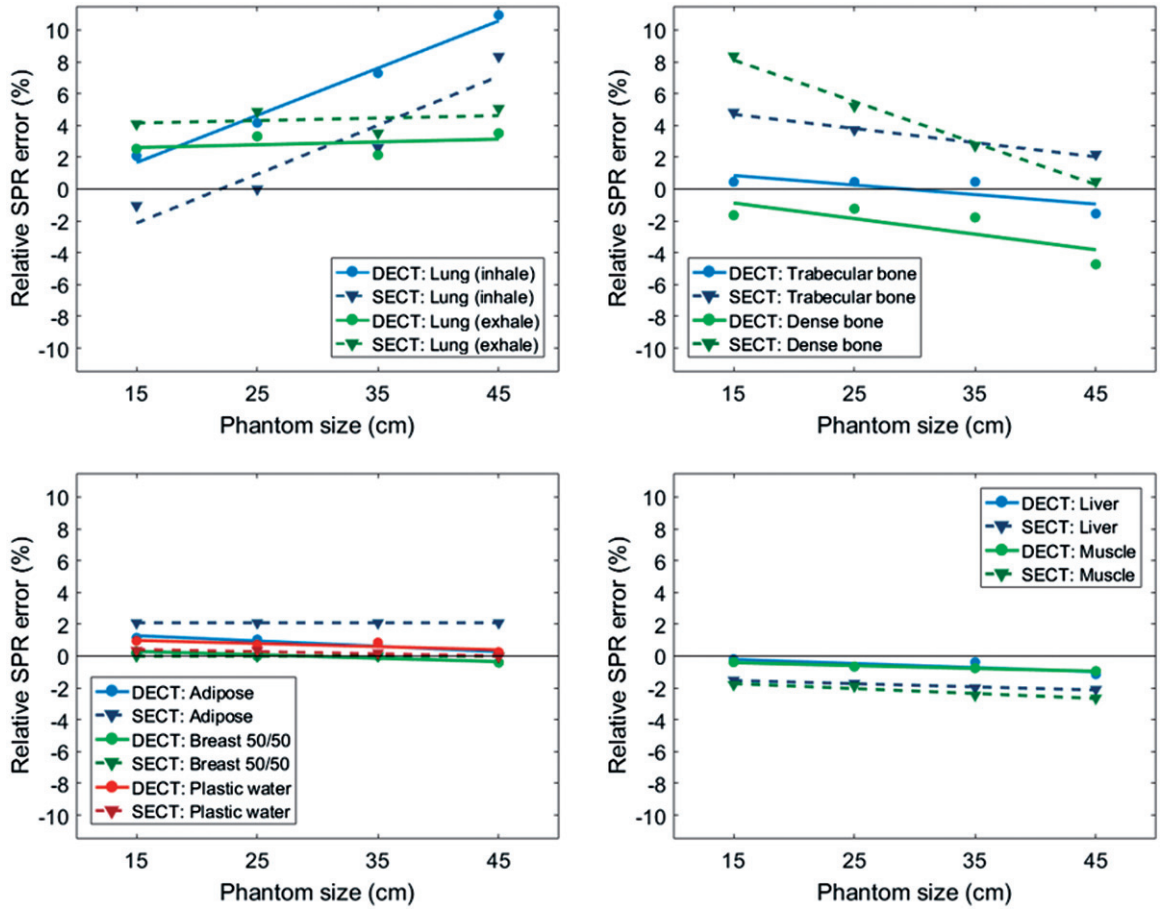

Figure 5. Percent error as a function of phantom size for all 10 materials for both SECT (triangles with dashed lines) and DECT (dots with solid lines).

Table 1. Relative proton stopping power (SPR) averaged over phantom size and material-specific coefficient of variation.

	Reference	Single energy			Dual energy		
Material	SPR	Mean	SD	CV	Mean	SD	CV
Lung (inhale)	0.192	0.197	0.008	4.1%	0.204	0.007	3.64%
Lung (exhale)	0.513	0.536	0.004	0.69%	0.528	0.003	0.63%
Adipose	0.957	0.977	0.000	0.00%	0.965	0.005	0.47%
Breast	0.983	0.983	0.000	0.0%	0.983	0.003	0.29%
Plastic water	0.995	0.997	0.002	0.19%	1.002	0.003	0.31%
Muscle	1.049	1.03	0.003	0.27%	1.043	0.004	0.42%
Liver	1.058	1.035	0.004	0.43%	1.051	0.003	0.24%
Trabecular bone	1.1	1.137	0.013	1.12%	1.099	0.011	1%
Dense bone	1.459	1.52	0.049	3.25%	1.425	0.023	1.64%

Using the Rho-Z software, SPR estimates were 0.936, 0.936 and 0.924 in the 25-, 35- and 45-cm tank, respectively. These estimates resulted in errors of 0.18%, 0.17% and −1.11%, respectively.

Discussion

Our study demonstrated that, for the CIRS materials, the DECT Rho-Z software produced SPR estimates that meet the same accuracy standards as the SECT stoichiometric method. However, the DECT Rho-Z approach does not require a calibration protocol by the user such as that required for SECT.

Regression analysis of the dataset as a whole did not indicate that SECT or DECT was superior in stabilizing SPR estimates across patient size, nor did it reveal an overall systematic bias with either technique. Likewise, material-specific regression analysis indicated a similar pattern concerning size dependence. However, the significant technique terms for dense bone and liver indicate that there is potentially systematic bias if SECT is used to quantify SPR in these tissues, but not when DECT is used. This is also evident in Figure 5 as nonzero intercepts for these materials.

Measurements of the silicone implant illustrate the superiority of using DECT versus SECT when nonbiologic materials are present. The presence of nonbiologic materials is the major disadvantage to using the stoichiometric method, as materials which do not comprise the calibration curve can be incorrectly characterized. In our study, this was illustrated by a mean absolute percent error in SPR of 11.46%, which exceeds the range uncertainty margin of 3.5% typically used to account for SPR estimation errors [17]. In a clinical scenario, this necessitates measurement of this material in a proton beam, and revision of the CT numbers in the SECT patient images in order to correctly estimate the WET. This can greatly add to the complexity of both the treatment planning process and the treatment itself. The Rho-Z estimates reduced this error to 0.49%, which is well within the acceptable range for treatment planning.

Limitations of our study include our analysis of the lung and dense bone materials. As was previously stated, Z_{eff} estimates in lung were not obtained by the Rho-Z software, leading us to approximate the SPR using the ρ_e estimate. For lungs, the nominal SPR is only 0.192 during inhalation and

0.513 during exhalation. Therefore, small absolute SPR errors are a relatively large percentage of the reference value. However, since the SPR for lung is so low, on a practical level, these relatively large percentage errors may only translate into a small fraction of the water equivalent depth of the target tissue and therefore may not meaningfully affect the treatment plan. Additionally, phantom lung inserts are typically made from foam, which can vary in density depending on slice position. These factors could have affected both the SECT and the DECT measurements. Mobberly et al. [18] demonstrated that lung CT number accuracy could be improved with scatter correction in a dual-source setup. Our SECT technique did not employ scatter correction, which could account for some of the error. For the dense bone, the elemental composition data provided by the manufacturer indicated that there was a small percentage of Barium in the insert. The presence of this high-Z material may not be compatible with our DE calculations [10,19]. Given these potential complications with the phantom measurements, further investigations are warranted using phantoms from other manufacturers and/or organic materials taken from animal models.

We have shown that the use of DECT with the Rho-Z software tool for SPR estimation can meet or exceed the performance of the SECT stoichiometric technique across a range of phantom sizes. We also have shown that DECT can be used to correctly estimate the SPR in an implanted material with unknown chemical composition. DECT may therefore be used to reduce the need for complex, patient-specific planning with an SECT protocol when non-biological tissues are present, while maintaining treatment efficacy and safety standards.

Acknowledgments

The authors would like to acknowledge Adam Bartley from the Mayo Clinic Department of Biomedical Statistics and Informatics for his guidance on the statistical analysis of the data presented in this report.

Disclosure statement

No potential conflict of interest was reported by the authors.

Funding

Dr. McCollough receives industry grant support from Siemens Healthineers. Drs. Krauss and Halaweish are employees of Siemens Healthineers.

References

[1] van Elmpt W, Landry G, Das M, et al. Dual energy CT in radiotherapy: current applications and future outlook. Radiother Oncol. 2016;119:137–144.
[2] Schneider U, Pedroni E, Lomax A. The calibration of CT Hounsfield units for radiotherapy treatment planning. Phys Med Biol. 1996;41:111–124.
[3] Woodard H, White D. The composition of body tissues. Br J Radiol. 1986;59:1209–1219.
[4] White DR, Woodard HQ, Hammond SM. Average soft-tissue and bone models for use in radiation dosimetry. Br J Radiol. 1987;60:907–913.
[5] ICRU. Stopping Power and Ranges for Protons and Alpha Particles. ICRU Report. 1993;49.
[6] Woodard H, White D. Bone models for use in radiotherapy dosimetry. Br J Radiol. 1982;55:277–282.
[7] Yang M, Zhu XR, Park PC, et al. Comprehensive analysis of proton range uncertainties related to patient stopping-power-ratio estimation using the stoichiometric calibration. Phys Med Biol. 2012;57:4095–4115.
[8] Bichsel H. Passage of charged particles through matter. New York (NY): McGraw-Hill; 1972.
[9] Yang M, Virshup G, Clayton J, et al. Theoretical variance analysis of single- and dual-energy computed tomography methods for calculating proton stopping power ratios of biological tissues. Phys Med Biol. 2010;55:1343–1362.
[10] Hunemohr N, Krauss B, Tremmel C, et al. Experimental verification of ion stopping power prediction from dual energy CT data in tissue surrogates. Phys Med Biol. 2014;59:83–96.
[11] Michalak G, Grimes J, Fletcher J, et al. Technical note: improved CT number stability across patient size using dual-energy CT virtual monoenergetic imaging. Med Phys. 2016;43:513–517.
[12] Wohlfahrt P, Mohler C, Hietschold V, et al. Clinical implementation of dual-energy CT for proton treatment planning on pseudo-monoenergetic CT scans. Int J Radiat Oncol Biol Phys. 2017;97:427–434.
[13] Bar E, Lalonde A, Royle G, et al. The potential of dual-energy CT to reduce proton beam range uncertainties. Med Phys. 2017;44:2332–2344.
[14] Landry G, Seco J, Gaudreault M, et al. Deriving effective atomic numbers from DECT based on a parameterization of the ratio of high and low linear attenuation coefficients. Phys Med Biol. 2013;58:6851–6866.
[15] Johns HE, Cunningham JR. The physics of radiology. Thomas CC, editor; 1983.
[16] Sternheimer RM, Seltzer SM, Berger MJ. Density effect for the ionization loss of charged-particles in various substances. Phys Rev B. 1982;26:6067–6076.
[17] Paganetti H. Range uncertainties in proton therapy and the role of Monte Carlo simulations. Phys Med Biol. 2012;57:R99–117.
[18] Mobberley SD, Fuld MK, Sieren JP, et al. Scatter correction associated with dedicated dual-source CT hardware improves accuracy of lung air measures. Acad Radiol. 2013;20:1334–1343.
[19] Mohler C, Wohlfahrt P, Richter C, et al. Methodological accuracy of image-based electron density assessment using dual-energy computed tomography. Med Phys. 2017;44:2429–2437.